True Time-Delay Fiber-Optic Control of an Ultrawideband Array Transmitter/Receiver with Multibeam Capability

Michael Y. Frankel and Ronald D. Esman, *Member, IEEE*

***Abstract*—A true time-delay beamformer based on a fiber-optic dispersive prism is developed and characterized. The beamformer is used to control an ultrawideband time-steered array antenna, which is a significant improvement over inherently narrowband phased-array antennas. The time-steered transmitter antenna consists of eight broadband spiral elements in a sparsely-populated array. In transmit mode the bandwidth is microwave-component limited to 2–18 GHz. The transmitter shows an unprecedented performance with $>100^\circ$ azimuth steering and no observed squint over the full frequency range. We also extend the beamformer functionality and demonstrate, we believe for the first time, fully-independent dual-beam dual-frequency ultrawideband antenna transmitter operation. Furthermore, the beamformer is shown to be capable of controlling the transmitter under pulsed operation with microwave pulse-widths as short as 75 ps. In the phase-steered receive mode, the antenna is component-limited to two elements and a frequency range of 6–16 GHz. However, we can still demonstrate squint-free receiver steering over $>70^\circ$ azimuth over the full available frequency range.**

I. Introduction

PHASED-ARRAY antennas (PAA) have been the subject of intense recent development. The primary driving force has been the possibility of electronic beam steering with the concomitant advantages over mechanically-steered arrays (speed, reliability, etc.) [1]. Electronic control over individual PAA elements can also be used for beam shaping functions. Yet, all-electronic control systems possess a number of drawbacks that include among others size, weight, loss, susceptibility to electro-magnetic interference, and narrow instantaneous bandwidth. Optical control techniques can provide benefits in all of the above areas; yet the most important advantage may be in the ability of optical techniques to provide a true time-delay (TTD) capability necessary for squint-free wide instantaneous bandwidth array steering [2]. A variety of optical TTD techniques have been proposed [3]–[10]. All of these techniques have had only a limited practical application, if any, due to the demands for specialized component development, precision mechanical matching, limited bandwidth, and/or excessive power losses. Recently, we have developed and demonstrated a superior beamforming technique that is based on all commercially-available components, has potentially high stability and reliability, and minimizes power losses [11].

Here we describe an implementation and characterization of a time-steered array (TSA) antenna controlled by a TTD fiber-optic beamformer. The TSA terminology is preferred over a more conventional phased-array one as it more accurately describes the TTD nature of antenna control. We demonstrate transmit and receive modes of operation, as well as more advanced multiple beam-forming. The linear antenna is a sparsely-populated array with eight broadband spiral elements. In the time-steered transmit mode, the system shows a $\pm 53^\circ$ squint-free azimuth steering over a 2 to 18 GHz instantaneous bandwidth. In the phase-steered receive mode, the available microwave components limit the array to only two active elements over a 6 to 16 GHz frequency range and a $\pm 35^\circ$ azimuth steering. Fully-independent dual-beam dual-frequency operation is also demonstrated in the transmit mode. To our knowledge, neither such wideband nor optically-controlled multi-beam functions have ever been demonstrated before.

II. System Configuration and Characteristics

A. Array Antenna Design

We chose a linear array to demonstrate the TTD and multiple beam steering capabilities of the new fiber-optic beamformer. An extension to a two-dimensional steering system is straightforward [11], but would introduce unnecessary complexity into the demonstration systems. Our TSA was composed of eight matched commercial cavity-backed spiral elements with good radiating characteristics covering the 2- to 18-GHz frequency range [12].

For the element spacing, we selected a sparsely-populated unequally-spaced array design with consecutive elements separated by 7.5, 7.5, 7.5, 10, 10, 17.5, and 12.5 cm. Such element spacing provides the following advantages: 1) the interelement separation is sufficiently large to accommodate the 6.2-cm diameter spiral elements; 2) the grating lobes are suppressed to higher frequencies than would be possible with equally-spaced elements; 3) the effective antenna aperture is increased providing for a narrow main lobe width. As a trade-off, the sidelobe level is higher than for a conventional eight-element fully-populated array.

Manuscript received January 16, 1995; revised March 19, 1995. This work was supported by the Office of Naval Research.

The authors are with the Naval Research Laboratory, Code 5672, Washington, DC 20375-5338

IEEE Log Number 9413686.

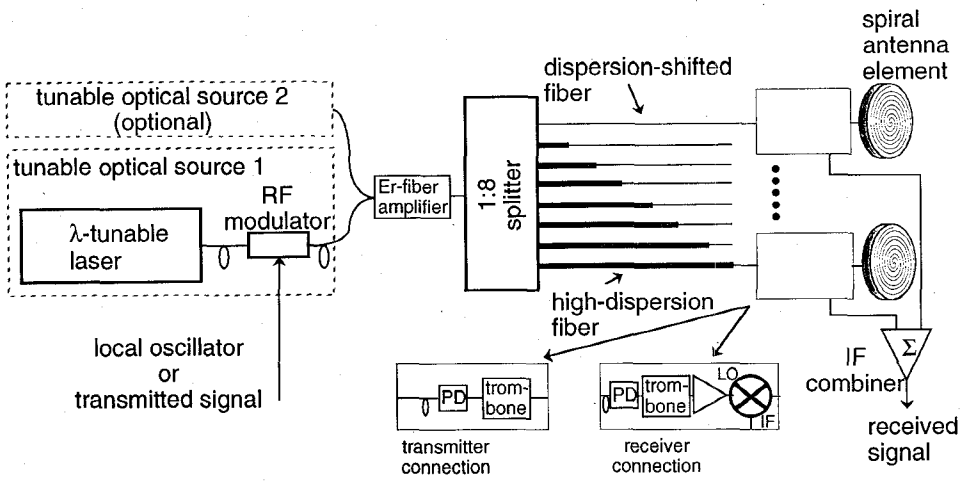

Fig. 1. Time-steered array antenna characterization system diagram.

The phased-array antenna radiated field can be obtained from a well known relation [13, p. 19]

$$F[u] = \sum_{n=\langle N\rangle} \left(|a_n| e^{-j\frac{d_e}{c} n\omega u_o}\right) e^{j\frac{d_e}{c} n\omega u} \tag{1}$$

where N is the number of elements in the array, $a_n = |a_n| e^{-j\frac{d_e}{c} n\omega u_o}$ is the signal radiated by element n, d_e is the interelement spacing, ω is the radiated signal radian frequency, and u is the sine space variable related to the mechanical angle Θ off normal to the array plane by $u = \sin(\Theta)$, and u_o is the array steered angle off broadside. The array beam steering is accomplished by introducing a microwave time-delay for the n-th element in the array given by

$$\tau_n = \frac{d_e}{c} u_o n. \tag{2}$$

For our TSA, the smallest common unit spacing increment is $d_e = 2.5$ cm. So, we can treat the TSA as having a total of 30 elements, but only the elements numbered (by position) 1, 4, 7, 10, 14, 18, 25, and 30 are active and have nonzero signal amplitudes a_n.

It should be noted that (1) is a Fourier synthesis equation applied to the signal distribution at the array aperture. Likewise, having measured the (discretized) array field pattern $F[u]$ at a certain frequency ω, we can similarly compute the array aperture signals from an inverse Fourier transform of the array field pattern as

$$a_n = \frac{1}{N} \sum_{u=\langle N\rangle} F[u] e^{-j\frac{d_e}{c} n\omega u}. \tag{3}$$

B. Fiber-Optic Beamformer Design and Operation

The fiber-optic beamformer is based on the principle of a dispersive fiber-optic link [9], with the beamformer configuration improved to simplify the TSA control function [11]. In brief, the microwave signal driving the antenna elements is transmitted on a single wavelength-tunable optical carrier via a bank of dispersive fiber-optic links. The TTD function is realized by tuning the carrier wavelength to vary the group velocity of the propagating signal. As seen from (2), each element requires a time-delay proportional to its relative position within the array. Thus, each fiber-optic link feeding an individual array element incorporates an overall amount of dispersion that is proportional to the element position. A set change in the carrier wavelength provides the necessary proportional time-delay for all array elements with a single wavelength-control input. This system is illustrated in Fig. 1.

Our bank of fiber-optic links was based on a combination of high-dispersion (HD) fiber [14] ($D_{\rm hd} \sim -70$ ps/nm·km) and dispersion-shifted (DS) fiber ($D_{\rm ds} \sim 0$ ps/nm·km). Then, for a signal of wavelength $\lambda = \lambda_o - \Delta\lambda$ we can compute the time-delay *change* relative to the delay at a reference wavelength λ_o. Assuming a link containing n units of HD fiber of length $\ell_{\rm hd}$ and $\ell_{\rm link} - n\ell_{\rm hd}$ meters of DS fiber, the time-delay *change* is given by

$$\begin{aligned}\Delta\tau_{\rm link} = {} & l_{\rm link}(D_{\rm ds}\Delta\lambda + D'_{\rm ds}(\Delta\lambda)^2) \\ & + n l_{\rm hd}\Delta\lambda((D_{\rm hd} - D_{\rm ds}) + \Delta\lambda(D'_{\rm hd} - D'_{\rm ds}))\end{aligned} \tag{4}$$

where the dispersion may vary linearly with wavelength as $D_{\rm hd} + D'_{\rm hd}(\lambda - \lambda_o)$ and $D_{\rm ds} + D'_{\rm ds}(\lambda - \lambda_o)$ for the HD and the DS fiber, respectively. The link $\Delta\tau_{\rm link}$ is given by a sum of one term which is common to all links (and may be ignored) and another term which is proportional to the link number n. Equating (2) and the second term of (4), we can obtain the required unit length of HD fiber. For our system, we require $\pm 60°$ beam steering capability with a maximum carrier wavelength deviation of $\Delta\lambda_{\rm max} \approx \pm 22.5$ nm, which gives $l_{\rm hd} \approx 46$ m. The consecutive links in our system contained nominal sections of 0, 138, 276, 414, 598, 782, 1104, 1334 m of HD fiber and were length-equalized to 1350 m with DS fiber.

The HD fiber length was measured with a mechanical counter to within ± 0.25 m. This error results in under a ± 1 ps *relative* delay error among the links (from second term of (4)). The overall delay was equalized by trimming the DS fiber to within ± 0.5 cm of the required length at a center wavelength of $\lambda_o = 1558$ nm. The final delay equalization to within ± 5 ps was accomplished via microwave trombone delay lines.

The long lengths of fiber present a thermal stability problem via changes in fiber physical length due to expansion and

optical length due to refractive index variations [15]. The refractive index thermal slope dominates the thermally-induced time delay variation and, for our links, amounts to $\Delta\tau_{\text{link}} \approx 54$ ps/°C, which accounts for most delay errors and calibration stability problems. Therefore, the fiber-optic beamformer was placed in an insulated enclosure, which served as an effective countermeasure.

The laser driving the beamformer was a fiber-optic tunable σ-laser (based on all commercially-available components) [16]. The laser was tunable from under 1530 nm to over 1580 nm with a 0.06-nm linewidth (implying more than 800 resolvable wavelength settings) and single-polarization output. The laser wavelength tuning speed was limited to the millisecond range by the Fabry-Perot etalon filter, but microsecond tuning speeds have been demonstrated with lasers including an acousto-optic filter [17]. The laser output was amplitude-modulated by a Mach-Zehnder (M-Z) modulator, amplified in an Er-fiber amplifier, and split into eight fiber-optic dispersive links. The outputs of the links were fed to individual photodetectors (PD's) followed by microwave trombones for time-delay calibration. For transmit-mode operation, the trombone outputs were fed directly to the corresponding antenna elements. For receive-mode operation, the trombone outputs were amplified and fed to RF-mixer local-oscillator (LO) ports. The antenna element outputs were connected to the RF-mixer RF ports. The benefit of the second (optional) tunable optical source is explained in Section III.

The amplitudes of the RF signals from each link were matched by introducing controlled bend loss into the fiber to provide frequency-independent attenuation. The RF spectral amplitude uniformity among all the links was acceptable over the complete 2- to 18-GHz frequency range. In addition to the customary small variability in performance ($\sim \pm 0.2$ dB) due to microwave component differences, there were two additional deleterious effects present. The first is an abnormally large ~2–3 dB gain and ~15° phase ripple across the whole band due to the mismatch between the high output impedance of the PD's and the 50-Ω impedance of the following microwave elements. This ripple could be eliminated in an improved system by either properly terminating the PD's or by inserting broadband isolators after the PD's. The second error is intrinsic to dispersive fiber-optic links and originates from microwave sideband phase walk-off at high modulation frequencies [18], [19]. This leads to a microwave loss on the order of ~3 dB at 18 GHz for the most dispersive link in our system, but is much smaller at lower frequencies and in less dispersive links. Therefore, the array pattern distortion is believed to be dominated by the array element coupling and by the PD mismatch ripple.

Additional systematic errors may arise from wavelength-dependent effects in the fiber-optic system. The pattern distortion introduced by these errors appears to be insignificant for our system, but may become a problem for low-sidelobe systems.

The optical link parameters, including optical and RF signal amplitudes and losses, can be summarized as follows. The M-Z modulator had an experimentally-deduced V_π of ~20 V and the optical power output of 0.3 mW. The 1 : 8 splitter loss of 9.55 dB (0.52-dB insertion loss), optical fiber loss of 3 dB, and the PD responsivity of 0.6 A/W combined to produce an overall 80 dB RF insertion loss for a single link. When all the PD RF outputs were combined in-phase, the overall RF insertion loss decreased to 62 dB. An addition of an Er-amplifier to the 1 : 8 splitter optical feed further reduced the overall insertion loss to ~40 dB, a loss commensurate with the modulator V_π and PD current of 0.15 mA.

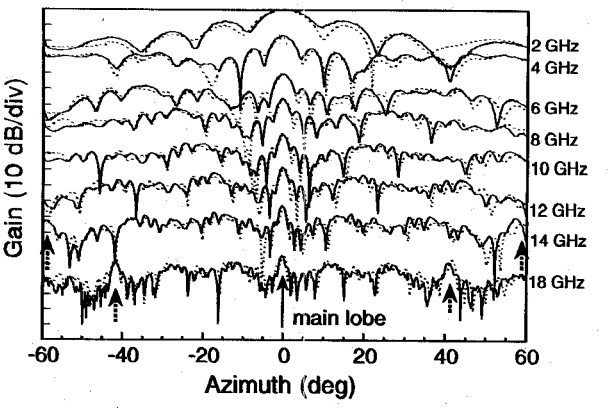

Fig. 2. Comparison between RF-fed (dashed) and optically-fed (solid) corrected antenna patterns. Dashed arrows indicate grating lobes.

III. Antenna Transmit-Mode Operating Characteristics

A. Transmit Mode Patterns

The array antenna patterns were measured in an anechoic compact radar range. A network analyzer under computer control was used to drive the M-Z modulator and to measure the received signal power and phase as a function of the antenna mechanical azimuth. Fig. 2 shows a comparison between RF-fed (dashed) and optically-fed (solid) TSA patterns with relative element timings adjusted for broadside transmission. The signals driving the element for the RF-fed array were verified to be within 0.2 dB in amplitude and within ~5° in phase over the complete 2 to 18 GHz frequencyrange. The RF-fed case thus represents a nearly best-case pattern under the constraints of the element coupling, element gain, and compact range characteristics. Of course, the RF-fed antenna could not be conveniently steered. The optically-fed TSA pattern, obtained with the laser tuned to $\lambda_o = 1558$ nm for broadside transmission, shows a reasonably good agreement with the best-case pattern over the complete 2- to 18-GHz frequency range. This comparison emphasizes that the interelement amplitude and phase mismatch errors do not significantly affect the TSA pattern for our system.

An ideal calculated pattern provides a benchmark for comparison to optically-steered array patterns that are corrected to account for the measured element gain. When the laser wavelength is detuned from the center one of λ_o, the array is steered off broadside. For example, Fig. 3 shows a comparison between corrected measured TSA pattern and ideal calculated one for a laser wavelength detuned by $\Delta\lambda = -10$ nm without any other adjustments. The main lobe steer angle is $-24°$

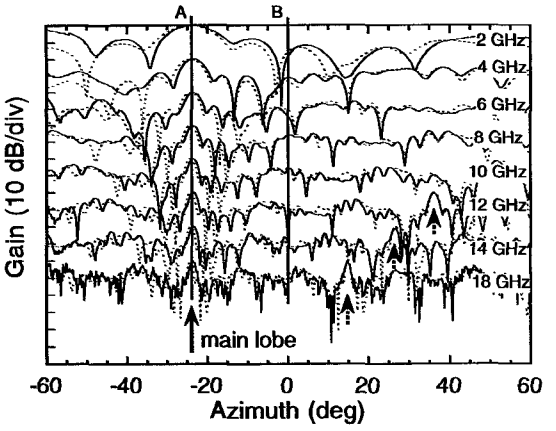

Fig. 3. Comparison between the corrected measured array pattern (solid) and ideal calculated one (dashed) for a laser wavelength detuned by $\Delta\lambda = -10$ nm for $-24°$ steering. Dashed arrows indicate grating lobes.

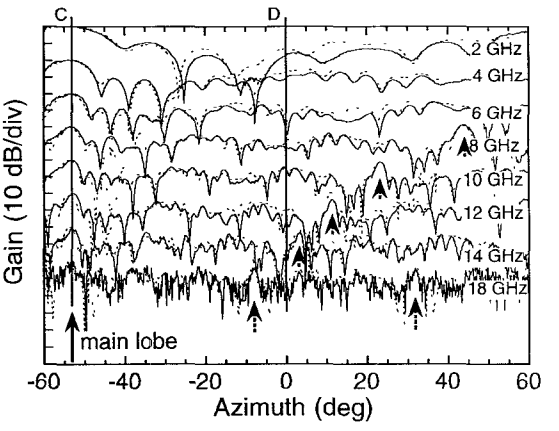

Fig. 4. Comparison between the corrected measured array pattern (solid) and ideal calculated one (dashed) for a laser wavelength detuned by $\Delta\lambda = -20$ nm for $-53°$ steering. Dashed arrows indicategrating lobes that appear above 8 GHz.

off broadside and is independent of frequency in the 2- to 18-GHz range, as expected for a TTD beamformer. Despite the measured mismatches and associated ripple in frequency-dependent parameters (see Section II), the agreement is seen to be good over the whole 2- to 18-GHz range. In general, we observe a narrowing main lobe, and sidelobes converging toward the main lobe with increasing frequency, as expected. The side lobe level is over 10 dB below the main lobe in its vicinity and rises up to ~5 dB below far off the main lobe. The measured nulls are as deep as 40 dB, indicating a reasonable amplitude and phase uniformity across the array. The grating lobes are absent in the data up to 12 GHz but appear in the higher frequency patterns (dashed arrows). The sidelobe levels, beamwidth, and grating lobes are all in agreement with the sparsely-populated unequal-spacing array design.

For comparison, a phase-steered PAA yields main lobe squint from ~8° to over 35° as the frequency is scanned from 18 GHz to under 4 GHz.

The limits of the optically-controlled beam steering can be explored by detuning the laser wavelength by $\Delta\lambda = -20$ nm. Fig. 4 shows a comparison between the corrected measured TSA pattern and ideal calculated one. The main lobe is steered to $-53°$ off broadside and its position is independent of frequency in the 2- to 18-GHz range. As before, the match between the measured and calculated patterns is good over the whole range of parameters. The signal-to-noise ratio (SNR) of the 18-GHz data is low due to the low optical power at the wavelength tuning limits of the laser.

Similar steering data can be obtained for wavelength detuning $\Delta\lambda$ ranging from -20 nm to $+20$ nm for beam steering from $-53°$ to $+54°$ off broadside, with the slight asymmetry due to the nonzero dispersion slope of the HD ($D'_{\rm hd} \neq 0$) and DS ($D'_{\rm ds} \neq 0$) fiber. Our TSA transmitter shows a 2- to 18-GHz bandwidth squint-free steering over a >100°–azimuth range.

B. Aperture Pattern from Antenna Pattern

As noted in Section II, the radiated signal distribution at the antenna aperture can be obtained from the measured array field pattern via (3). Since both power and phase were measured, all the necessary information is available. However, the measured phase must be compensated for the antenna rotation center being displaced from its aperture plane center. The rotation compensation was applied to the corrected measured broadside pattern at 8 GHz and the calculated aperture signal amplitude distribution is shown in Fig. 5. The aperture distribution is shown for 50 equivalent element spacings d_e, as described in Section II. The largest signals correspond to the actively-driven elements at positions 1, 4, 7, 10, 14, 18, 25, and 30, which match the actual element positions. These signals are uniform to within 2 dB indicating good driving signal amplitude match. The nonzero signals from other "virtual" elements may be attributed to the array pattern distortion due to the incomplete correction for the element gain, element mutual cross-coupling, and compact range effects.

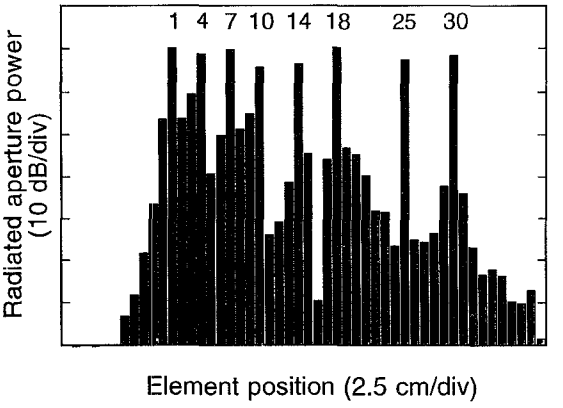

Fig. 5. A perturesignal power distribution calculated from the 8-GHz broadside corrected array pattern.

C. Frequency-Domain Data

The array pattern synthesis (1) indicates that the pattern dependence on the signal frequency ω and on the sine space angle u is functionally identical. The array pattern obtained by mechanically scanning the azimuth at some nonzero frequency ω may also be obtained by sweeping the frequency at some array angle u. The TSA patterns would be identical under

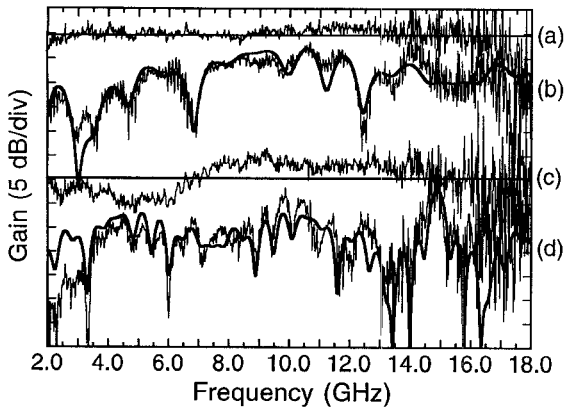

Fig. 6. Frequency-domain sweeps with antenna mechanical azimuth and optical steering settings as parameter. (a) $\Delta\lambda = -10$ nm, $\Theta = -24°$ off broadside; (b) $\Delta\lambda = -10$ nm, $\Theta = 0°$ on-broadside; (c) $\Delta\lambda = -20$ nm, $\Theta = -53°$ off broadside; (d) $\Delta\lambda = -20$ nm, $\Theta = 0°$ on-broadside.

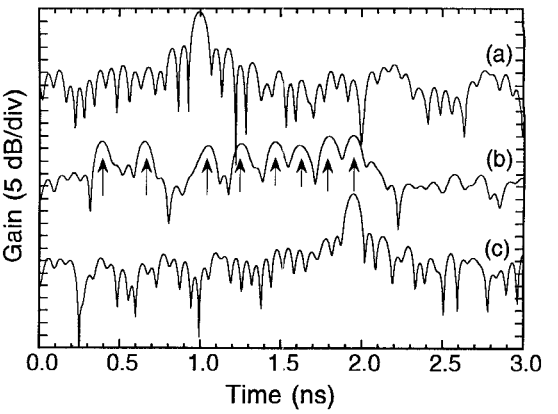

Fig. 7. Synthesized time-domain impulse-response with antenna mechanical azimuth and optical steering setting as parameter (a) $\Delta\lambda = -0$ nm, $\Theta = 0°$ on-broadside; (b) $\Delta\lambda = 0$ nm, $\Theta = -40°$ off broadside, expected "minor" pulse arrival times are shown by arrows; (c) $\Delta\lambda = -16.3$ nm, $\Theta = -40°$ off broadside.

ideal conditions only, and any perturbation introduced by the microwave component frequency response, element gain, and compact range characteristics would introduce pattern distortions. The frequency-domain sweep is equivalent to a measurement performed along the vertical section lines A, B, C and D as indicated in Figs. 3 and 4.

Fig. 6 shows frequency-domain sweeps for several TSA mechanical azimuth and optical steering settings. The microwave component frequency responses were calibrated out by a sweep at TSA broadside settings. However, the element coupling and gain and the compact range effects could not be conveniently accounted for. Curve (a) shows a sweep for a mechanical angle of $-24°$ and the wavelength detuned by -10 nm. This is equivalent to a sweep along Section A in Fig. 3 along the main lobe peaks, and the result is a nominally flat response. Curve (b) shows a sweep for a mechanical angle of $0°$ and the wavelength detuned by -10 nm. This is equivalent to a sweep across Section B in Fig. 3 across many sidelobe peaks and nulls, and the result is an oscillating (but predictable) frequency response. The agreement to calculations, shown as thick lines, is good. Similarly, curves (c) and (d) show sweeps for the wavelength detuned by -20 nm and mechanical angles of $-53°$ and $0°$ corresponding to sections C and D in Fig. 4 respectively. The agreement with the calculations is good, but somewhat degraded by the wavelength and element gain pattern effects.

An interesting application of this tunable frequency-dependent power can be realized by implementing a tunable tapped delay-line microwave finite impulse response filter [20].

D. Time-Domain MicrowaveImpulse Response

The available equipment did not allow us to evaluate the time-domain impulse response of the TSA transmitter. Still, the amplitude and phase data from the frequency-domain sweeps discussed in Section III present an opportunity to evaluate the TSA transmitter impulse response via an inverse Fourier transformation. Such transformation from the frequency domain into the time domain is valid only if the system is linear and time-invariant.

For our case, the measured frequency range covers a 16-GHz bandwidth. Assuming a top-hat spectral envelope, this bandwidth corresponds to a microwave pulse of 1.2/16 GHz = 75 ps full-width at half-maximum modulating the optical carrier. The dispersion-induced pulse spreading has been derived by Marcuse [21] and is negligible for 75-ps optical pulses even for the link with the highest dispersion in our beamformer. Hence, the fiber-optic beamformer does satisfy the linearity and the time-invariance requirements, and an inverse Fourier transform can be used to obtain an equivalent impulse response.

Fig. 7 shows the time-domain responses obtained for several antenna mechanical azimuth and optical steering settings with the microwave-component frequency response calibrated out. The top curve (a) is obtained when the array mechanical and optical steering is set for broadside and exhibits a "major" transmitted broadband pulse due to the temporal overlap (simultaneous arrival) of all the "minor" pulses radiating from the individual elements. When the array is mechanically rotated by $-40°$ off broadside while the optical steering is still set for broadside, there is an inherent time-delay introduced into the arrival time to the receiver of the "minor" pulses emitted from each one of the eight elements, and all eight pulses are clearly resolved (see curve (b)). These "minor" pulses are separated in time proportionally to the element spatial separation, and the expected pulse arrival times are indicated in the plot by arrows. Then, the mechanical angle is left at $-40°$ but the array is steered optically to that same angle by a wavelength detuning of $\Delta\lambda = -16.3$ nm. The "minor" emitted pulses are now optically time-delayed such that their arrival time to the receiver is simultaneous, and all eight pulses overlap temporally again [see curve (c)]. This "major" pulse is time-delayed relative to the broadside case due to the array rotation center not coinciding with the aperture plane and due to one-sided operation of the dispersive time-delay. That is, the one-sided operation cannot delay the arrival time for the elements on one side of the center and advance the arrival time for the other side. However, use of both normal and anomalous dispersion fiber would allow two-sided operation.

We believe that, though synthesized, such time-domain impulse data for the first time practically demonstrates a beamformer capable of steering ultrawideband pulsed antenna arrays.

E. Dual-Wavelength/Same Frequency Operation

The functionality of the beamformer can be extended significantly if active beam shaping is implemented. A practical application for a beam shaping function may be to implement a TSA operation with multiple beams. The antenna transmitter described in the above sections was controlled via microwave signal distribution on a single optical carrier. Our system allows a straightforward extension to multiple beam operation function simply by adding another independently-modulated and wavelength-tuned optical carrier (as shown in Fig. 1). Thus, we may realize simultaneous multiple-beam transmission at nearly arbitrary steering directions and frequencies.

In this section we discuss the implementation of a dual-beam transmitter with both beams at identical frequencies. In this case, the fiber-optic beamformer is fed by two independently wavelength-tunable and RF-modulated lasers, but both M-Z modulators are driven by the same microwave signal.

There are two potential problems that need to be addressed when operating in a dual-beam mode. The first potential problem is that the photodetection process is inherently nonlinear in converting from the optical carrier field to the output photocurrent. There will be potentially deleterious intermixing products among the two optical carriers and their microwave modulation sidebands. Under cw operation, which is our case, all detrimental intermodulation components will fall outside the receiver passband if $|\Omega_1 - \Omega_2| \neq 0$, $|\Omega_1 - \Omega_2| \neq \omega$, and $|\Omega_1 - \Omega_2| \neq 2 \cdot \omega$, where Ω_1 and Ω_2 are the optical carrier frequencies, and ω is the RF modulating frequency. Under pulsed operation, the receiver is assumed to be broadband and the intermodulation components can be filtered out and ignored if $|\Omega_1 - \Omega_2| > 2 \cdot \omega_{\max}$, where $\omega_{\max}$ is the maximum frequency contained in the modulating RF pulse. Orthogonal optical carrier polarizations may also be used to relax the restrictions if only two beams with a narrow wavelength separation are present.

The second potential problem is similar in that the power transmitted at some angle Θ is related to the square of the radiated field amplitude. Under cw operation, if the fields radiated in response to the two carriers are exactly out of phase then there will be an interferometric null in that direction. This problem is minimized if one of the beams is steered to the direction corresponding to a low sidelobe of the other beam.

To prevent the possibility of microwave destructive interference problems when the beams are steered close to each other, the microwave links are adjusted so that the time-delay for both signals is identical when both optical sources are set to the same $\Delta\lambda$. Fig. 8 shows the array patterns obtained with the dual independent beam steering system, with Fig. 8(a) showing two beams steered to broadside and $-28°$ off broadside via optical carriers at 1558 and 1546 nm, respectively, and Fig. 8(b) showing two beams steered to $-13°$ and $-28°$ off broadside via optical carriers at 1552 and 1546 nm respectively. The independent dual-beam squint-free steering is clearly demonstrated. The poor contrast between the main lobe and the sidelobes is because our sparsely-populated antenna has sidelobes only 5 dB down *by design*. The laser output power, and consequently the RF signal power, varies with wavelength. Therefore, the optical power had to be readjusted for each wavelength pair to produce an approximately equal RF power from both carriers. Otherwise, the main lobe level of one beam could fall below the high sidelobe level of the other beam. The poor SNR at higher frequencies is due to the steep gain rolloff of the microwave components and the sharing of the Er-fiber amplifier by both optical beams.

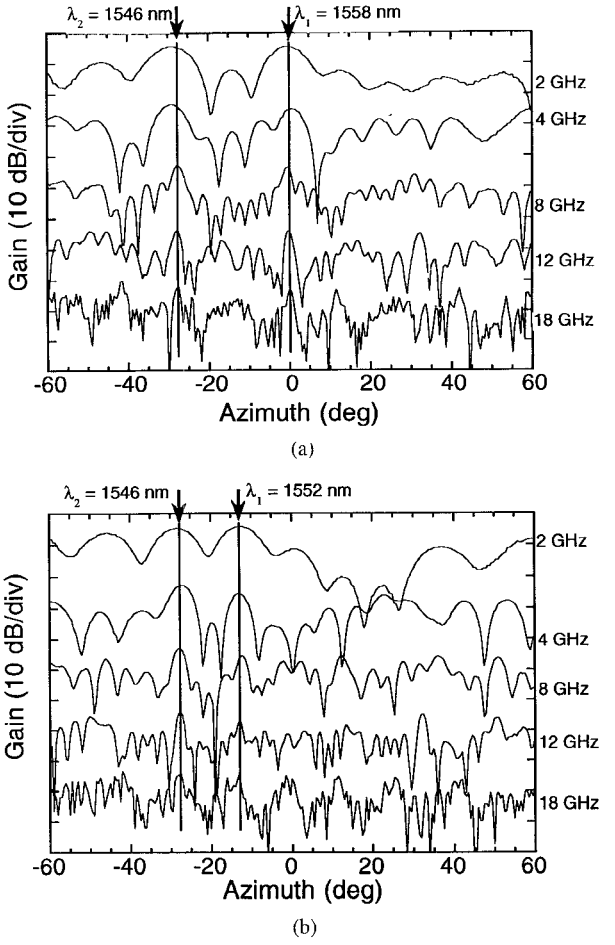

Fig. 8. Array patterns obtained with the independent dual-beam single-frequency steering system. (a) $\lambda_o$and $\Delta\lambda = -12$ nm optical settings for broadside and $-28°$ off-broadside beam steering. (b) $\Delta\lambda = -12$ and $\Delta = -6$ nm optical settings for $-13°$ and $-28°$ off-broadside beam steering.

The inverse Fourier transformation could be applied to the frequency-domain sweep data to obtain the impulse response data as for the case of a single beam (Section III). The difference being that now there are two independently-controlled sets of time-domain pulses that can be made to separate or overlap.

F.Dual-Wavelength/Dual Frequency Operation

A further extension of the dual-beam identical-frequency operation is a dual-beam dual-frequency operation. This op-

eration may still have a problem due to the detection of the intermixing products of the optical carriers, but since the network analyzer detection is narrowband, it is not expected to be of practical consequence. To verify this, we measured the TSA transmit patterns with one radiated signal frequency as a parameter and second signal frequency fixed at 4 GHz, which is not phase-locked with the first frequency. The antenna mechanical azimuth and both optical settings were adjusted for broadside transmission. We observed that all the patterns are similar to the ones shown in Section III and indicate no visible distortions with one exception: the antenna pattern at 4 GHz is completely washed out by the second interfering (jamming) signal.

Section III describes the squint-free TSA antenna radiation patterns and the synthesized ultrawideband impulse response under fully independent dual-beam dual-frequency operation. We believe that such beamformer functionality has never been demonstrated before. Flexible beam shaping and beam nulling could be accomplished using many laser wavelengths or by using a spectrally-shaped (and dynamically-reconfigurable) broadband optical source.

IV. Antenna Receive Mode Operating Characteristics

The same fiber-optic beamformer that was used to control the TSA in transmit mode can be used to control the array in the receive mode. In the receive configuration, the beamformer generates properly phased local oscillator (LO) signals for downconverting the signals received by the antenna elements. The optical wavelength settings required for receive-mode steering are complementary to the transmit mode, in the sense that a time-delay required in one mode corresponds to a time-advance in the other. Fortunately, such operation is easily achieved in our system simply by tuning the wavelength to the opposite side of the center wavelength λ_o.

The receive-mode system connection is described in Section II. The downconverted IF signals are combined and fed into the microwave receiver for measurement. The LO and RF signals were offset by 20 MHz from each other in our experiments. The availability of microwave mixers and high-gain matched RF amplifiers has limited our array to only two elements in the receive mode. Also, the matched amplifiers available to us have limited the operating frequency range to 6 to 16 GHz.

The receive patterns were obtained by using fiber-optic links #1 (no HD fiber) and #8 (1334 m of HD fiber) to provide the LO signals to array elements separated by 10 cm; the undriven array elements were passively terminated. Since there were only two active elements in the array, this driving arrangement ensured a reasonable number of grating lobes over the scanned azimuth range with a reduced required laser wavelength detuning.

Fig. 9 shows the array antenna patterns with the laser set at λ_o for broadside reception. For the two-element array there is no main lobe that can be differentiated by a larger amplitude, there are no sidelobes, and all the grating lobes are of equal amplitudes. The SNR is worse for the receive case due to a poor mixer conversion efficiency. Still, we observe

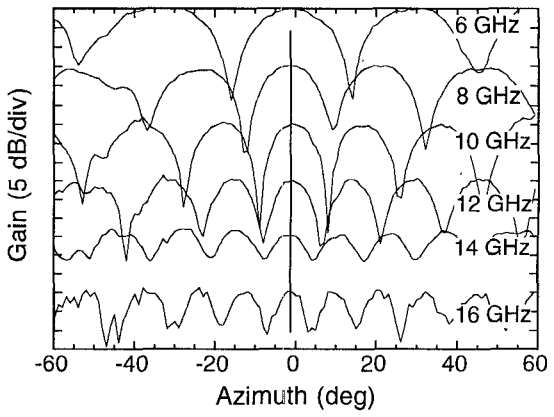

Fig. 9. Array pattern with the laserset at $\lambda_o = 1558$ nm for reception from broadside.

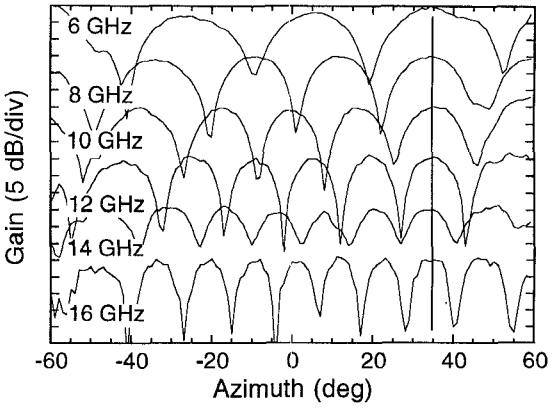

Fig. 10. Array pattern with the laser wavelength detuned by $\Delta\lambda = -2$ nm forreception from + off broadside.

a frequency-independent "main" lobe positioned at broadside ($\Theta = 0°$), with its width narrowing with increasing frequency.

As for the transmit case, the broadband steering is demonstrated simply by tuning the laser wavelength. The receive mode requires a wavelength detuning which is complementary to the transmit case. For example, to receive from a $+10°$ the laser wavelength would have to be set to the one required for transmission at $-10°$. Fig. 10 shows the array antenna pattern with the laser wavelength detuned by -2 nm and the nominal main lobe steered to $+35°$. The main lobe position is observed to be frequency-independent within the measurement resolution indicating proper LO phases. As for the broadside case, the nulls and the grating lobes converge toward the main lobe with increasing frequency. Similar steering patterns were obtained with the laser detuned by $+2$ nm for receive steering to $-35°$, as well as other wavelength settings for intermediate angle steering.

As for the transmit case, a frequency-domain sweep can be performed to obtain a response similar to the array pattern measurement without mechanical azimuth rotation. The measured results followed the expected two-element interference pattern.

V. Summary

We have developed and demonstrated a novel dispersive fiber-optic TTD beamforming system for phased-array antenna

control applications. The optical sources and the beamformer itself are constructed from all commercially-available components requiring no specialized development. The system is rugged, lightweight, immune to electro-magnetic interference, and potentially low-cost and reliable. A single low-voltage control signal is used to set the radiation steering angle, with the potential number of resolvable steering angles exceeding 800. The beamformer was used to time-steer a broadband eight-element linear sparsely-populated array. The system has demonstrated TTD squint-free steering over the 2 to 18 GHz frequency range across a $>100°$ azimuth range in the transmit mode. The antenna aperture signals provided via a fiber-optic feed were shown to be sufficiently uniform based on comparisons to an RF-fed antenna, as well as by calculation from the measured antenna patterns. The transmitter also shows a synthesized equivalent 75-ps impulse response capability. Furthermore, the beamformer versatility was illustrated by demonstrating a transmitter system with two independently-steerable beams of nearly arbitrary frequencies. The same beamformer was used to drive a two-element array in the receive mode with a demonstrated steering over a $>70°$ azimuth in the 6- to 16-GHz frequency range. The receive mode could be converted to a TSA configuration by having the receive signals traverse the same dispersive prism architecture [9]. The beamformer can be extended to the two-dimensional array applications in a straightforward manner without introducing excessive complexity. We believe that our time-steered antenna system demonstrates a number of breakthrough performance characteristics that include squint-free transmitter steering over more than three octaves at high-frequencies corresponding to a 75-ps time resolution, fully-independent dual-beam dual frequency transmitter operation, and wide frequency range receiver steering.

ACKNOWLEDGMENT

The authors would like to thank M. G. Parent and J. Valenzi for help in antenna pattern measurements, L. Goldberg and J. F. Weller for useful discussions and encouragement, and J. Dexter for providing crucial fiber-optic components and subsystems.

REFERENCES

[1] E. Brookner, *Practical Phased Array Antenna Systems*. Norwood, MA: Artech House, 1991.
[2] H. Zmuda and E. N. Toughlian, *Photonic Aspects of Modern Radar*. Norwood, MA: Artech House, 1994.
[3] E. N. Toughlian and H. Zmuda, "A photonic variable RF delay line for phased array antennas," *J. Lightwave Technol.*, vol. 8, no. 12, pp. 1824–1828, Dec. 1990.
[4] W. Ng, A. A. Walston, G. L. Tangonan, J. J. Lee, I. L. Newberg, and N. Bernstein, "The first demonstration of an optically steered microwave phased array antenna using true-time-delay," *J. Lightwave Technol.*, vol. 9, no. 9, pp. 1124–1131, Sept. 1991.
[5] D. Dolfi, F. Michel-Gabriel, S. Bahn, and J. P. Huignard, "Two-dimensional optical architecture for time-delay beam forming in a phased-array antenna," *Optics Lett.*, vol. 16, no. 4, pp. 255–257, Feb. 1991.
[6] A. P. Goutzoulis, D. K. Davies, and J. M. Zomp, "Hybrid electronic fiber optic wavelength-multiplexed system for true time-delay steering of phased array antennas," *Opt. Eng.*, vol. 31, no. 11, pp. 2312–2322, Nov. 1992.
[7] E. Ackerman, S. Wanuga, D. Kasemset, W. Minford, N. Thorsten, and J. Watson, "Integrated 6-bit photonic true-time-delay unit for lightweight 3–6 GHz radar beamformer," in *1992 IEEE MTT-S Dig.*, 1992, pp. 681–684.
[8] N. A. Riza, "Transmit/receive time-delay beam-forming optical architecture for phased-array antennas," *Appl. Opt.*, vol. 30, no. 32, pp. 4594–4595, Nov. 1991.
[9] R. Soref, "Optical dispersion technique for time-delay beam steering," *Appl. Opt.*, vol. 31, no. 35, pp. 7395–7397, Dec. 1992.
[10] W. D. Jemison and P. R. Herczfeld, "Acoustooptically controlled true time delays," *IEEE Microwave Guided Wave Lett.*, vol. 3, no. 3, pp. 72–74, Mar. 1993.
[11] R. D. Esman, M. Y. Frankel, J. L. Dexter, L. Goldberg, M. G. Parent, D. Stilwell, and D. G. Cooper, "Fiber-optic prism true time-delay antenna feed," *IEEE Photon. Technol. Lett.*, vol. 5, no. 11, pp. 1347–1349, Nov. 1993.
[12] Phase Matched Cavity Backed Spiral Antennas, *Model ASO-1503AAT*, AEL Defense Corp., Lansdale, PA.
[13] R. J. Mailloux, *Phased Array Antenna Handbook*. Norwood, MA: Artech House, 1994.
[14] A. J. Antos and D. K. Smith, "Design and characterization of dispersion compensating fiber based on the LP01 mode," *J. Lightwave Technol.*, vol. 12, no. 10, pp. 1739–1745, Oct. 1994.
[15] J. J. Carr, S. L. Saikkonen, and D. H. Williams, "Refractive index measurements on single-mode fiber as functions of product parameters, tensile stress, and temperature," *Fiber and Integrated Optics*, vol. 9, pp. 393–396, 1991.
[16] I. N. Duling, III and R. D. Esman, "Single-polarization fiber ampifier," *Electron. Lett.*, vol. 28, no. 12, pp. 1126–1128, June 1992.
[17] M. Y. Frankel, R. D. Esman, and J. F. Weller, "Rapid continuous tuning of a single-polarization fiber ring laser," *IEEE Photon. Technol. Lett.*, vol. 6, no. 5, pp. 591–593, May 1994.
[18] B. Christensen, J. Mark, G. Jacobsen, and E. Bodtker, "Simple dispersion measurement technique with high resolution," *Electron. Lett.*, vol. 29, no. 1, pp. 132–134, Jan. 1993.
[19] W. A. Wood, M. Y. Frankel, and R. D. Esman, "High-dispersion tunable optical delay line performance limits," in preparation for *IEEE Photon. Technol. Lett.*
[20] M. Y. Frankel and R. D. Esman, "Fiber-optic tunable microwave transversal filter," *IEEE Photon. Technol. Lell.*, vol. 7, no. 2, pp. 191–193, Feb. 1994.
[21] D. Marcuse, "Pulse distortion in single-mode fibers," *Appl. Opt.*, vol. 19, no. 10, pp. 1653–1660, May 1980.

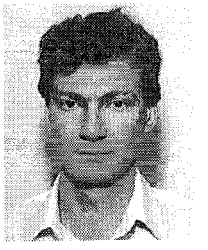

Michael Y. Frankel was born in St. Petersburg, Russia, in 1964. He received the B.S. degree (magna cum laude) from the University of Maryland, College Park, MD, in 1986, the M.S. degree from the University of Rochester in 1988, and the Ph.D. degree from the University of Michigan, Ann Arbor, in 1991, all in electrical engineering.

He is currently with the Optical Sciences Division, Naval Research Laboratory. His interests are in ultrafast optoelectronic studies and modeling of semiconductor materials, high-speed transmission lines, photodetectors, and transistors. He is also actively involved in developing fiber-optic components and control methods for phased-array radars. He has (co)authored over 30 publications and conference presentations in these areas and holds two patents.

Ronald D. Esman (M'85), for a photograph and biography, see this issue, p. 2213.